

Article

Fabrication and Photocatalytic Activity of Single Crystalline TiO₂ Hierarchically Structured Microspheres

Haisheng Huang^{1,2}, Qi Kong^{1,2}, Xin Yue^{1,2}, Kunlei Wang³ , Zhishun Wei^{1,2,4,*}  and Ying Chang^{1,2,4,*}

¹ Hubei Provincial Key Laboratory of Green Materials for Light Industry, New Materials and Green Manufacturing Talent Introduction and Innovation Demonstration Base, Hubei University of Technology, Wuhan 430068, China

² School of Materials and Chemical Engineering, Hubei University of Technology, Wuhan 430068, China

³ Institute for Catalysis, Hokkaido University, Sapporo 001-0021, Japan

⁴ Hubei Longzhong Laboratory, Xiangyang 441000, China

* Correspondence: wei.zhishun@hbut.edu.cn (Z.W.); cy0025@hbut.edu.cn (Y.C.)

Abstract: Single crystalline anatase TiO₂ microspheres with co-exposed {001}/{101} facets were prepared by a facile one-pot hydrothermal method using NaF as a morphology controlling agent. The influences of the NaF amount on the morphology and also on the photocatalytic activity were investigated systematically. The obtained microspheres possessed better morphology when the concentration of NaF was chosen at 0.1 mol/L, and the experimental results indicated that the crystal structure and morphology played important roles on the photocatalytic activity, based on the experimental results it was found that the photocatalytic degradation efficiency of TiO₂ microspheres on Tetracycline hydrochloride could reach 76.4% in 2 h. Finally, a growth mechanism was proposed by investigating the growth process, i.e., a synergistic effect of F ions modified Ostwald ripening and oriented attachment.



Citation: Huang, H.; Kong, Q.; Yue, X.; Wang, K.; Wei, Z.; Chang, Y.

Fabrication and Photocatalytic Activity of Single Crystalline TiO₂ Hierarchically Structured Microspheres. *Catalysts* **2023**, *13*, 201. <https://doi.org/10.3390/catal13010201>

Academic Editors: Detlef W. Bahnemann, Ewa Kowalska, Ioannis Konstantinou, Magdalena Janus, Vincenzo Vaiano, Wonyong Choi, Zhi Jiang and Yuanhua Sang

Received: 12 December 2022

Revised: 12 January 2023

Accepted: 13 January 2023

Published: 15 January 2023



Copyright: © 2023 by the authors. Licensee MDPI, Basel, Switzerland. This article is an open access article distributed under the terms and conditions of the Creative Commons Attribution (CC BY) license (<https://creativecommons.org/licenses/by/4.0/>).

Keywords: titanium dioxide; microsphere; hierarchical structure; mechanism; photocatalysis

1. Introduction

As one of the most potential photocatalyst, TiO₂ can be widely used in energy and environmental fields. However, due to its shortcomings, such as wide band gap, low quantum efficiency and difficulty in recycling nanoparticles, which limits its large-scale application. Many methods have been employed to improve the photocatalytic efficiency of TiO₂, e.g., ion doping [1–6], noble metal modification [7–11], semiconductor composite [12–17]. Ever since Yang [18] synthesized anatase TiO₂ single crystal with {001} crystal planes exposure rate of 47%, crystal plane control of TiO₂ has become a new means to effectively improve the photocatalytic activity of TiO₂ [19,20]. Afterwards, Li [21] increased the exposure rate of {001} crystal plane of anatase to 65%, and its photocatalytic activity was significantly higher than that of P25. Moreover, Liu [22] synthesized single crystals with co-exposed {001}/{110} crystal planes, and their photocatalytic activity was higher than that of irregular anatase TiO₂. Therefore, Yu [23] found that the TiO₂ with co-exposed {001} and {101} crystal planes was beneficial to the transfer and separation of photogenerated electrons and holes, then the theory of surface heterojunction was proposed, and it was believed that 55% of the exposed {001} was the optimal ratio. In addition to the {001} and {101} crystal facets, the {010} crystal facets of anatase have also attracted the attention of many researchers. Li [24] prepared anatase nanorods containing {010} crystal facet, which showed better photocatalytic activity than commercial anatase. Pan [25] also synthesized TiO₂ rod with dominant {010} surface and believed that excellent performance in converting CO₂ into CH₄ from its unique atomic structure and the lowest conduction band width. However, these research objects are mostly anatase single crystals, without the advantage of hierarchical structure. Based on the performance enhancements of hierarchical structure,

Xiang [26] synthesized flower-like TiO_2 films with co-exposed {001} and {101} crystal planes, and its selective photocatalytic degradation activity of azo dyes in water could be tuned by varying the degree of etching of {001} facets. Han [27] also prepared anatase microspheres with {001} exposed rate close to 100% on titanium foil, and its photoelectrocatalytic oxidation capability of Dimethylphthalate (DMP) wastewater was enhanced. Sayed [28] found that different pH and cations would significantly influence the degradation ability of TiO_2 microspheres film to norfloxacin. Zheng [29] has synthesized TiO_2 hierarchical microspheres, which have good crystal facets synergistic effect and hydrogen evolution activity. However, it is not environmentally friendly to use toxic chemicals (HF) to control the morphology of the films during the above-mentioned process. In addition, the above studies did not pay attention to the recyclability of samples, which limited the practical application. Therefore, there is an urgent requirement to find a safe and non-toxic [30] way to prepare the easy-to-recycle TiO_2 powders. In this study, the hierarchical structure anatase TiO_2 microspheres with co-exposed {001}/ {101} crystal planes were successfully prepared by one-pot hydrothermal method. The photocatalytic activity of the TiO_2 microspheres could be efficiently enhanced by co-exposed {001}/ {101} facets, and the recyclability could be significantly improved by larger particle size of the microsphere. Additionally, the formation mechanism of microspheres was proposed based on the investigation of the morphological variation at various growth conditions.

2. Results and Discussion

2.1. Structures and Morphology

Figure 1 shows the XRD patterns of the as-prepared powders treated with various NaF concentrations. All diffraction peaks were well indexed to the anatase structure of TiO_2 (PDF 01-084-1825). The sharp diffraction patterns indicated all the samples were well-crystallized anatase TiO_2 powders. With an increase in concentrations of NaF, the intensity and the width of anatase peaks were gradually changed to be stronger and narrower, and sample T3 deserved the highest crystallinity. However, further increase in NaF concentrations resulted in a slight decrease in intensity of anatase peaks, which indicated the NaF concentration had important influence on the crystalline phase and a suitable concentration of NaF was beneficial to forming well-crystallized anatase phase.

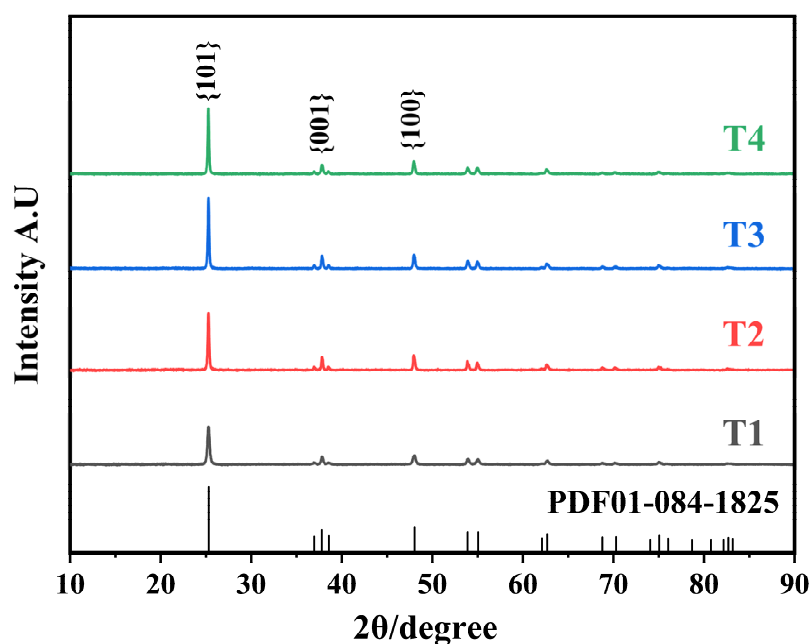


Figure 1. XRD patterns of samples treated with different NaF concentrations, denoted as T1, T2, T3 and T4, respectively.

Figure 2 showed the morphologies of samples prepared under various NaF concentrations (corresponding to Samples T1, T2, T3 and T4, respectively), which indicated that the NaF concentration had a significant influence on the size of the prepared samples. When the NaF concentration was 0.0667 mol/L, micron-sized spherical particles and irregular aggregates of non-spheres nano-sized nanoparticles coexisted in the product (as shown in Figure 2a,b), whose morphology was different from those of the powders synthesized at the other NaF concentrations. The morphology of nanoparticles was not uniform, and the particle size was about 20–100 nm (higher magnification could be seen in Figure S1). At the same time, a small part of particles was agglomerated into micron-sized spheroids, which indicated that those nanoparticles had the tendency to form spheres at this NaF concentration. Comparing with the samples prepared in other NaF concentrations, although XRD results showed that the crystalline form of these samples were anatase, only a few particles in the SEM images of sample T1 showed obvious characteristics of anatase {001}/{101} crystal facets. However, the decahedral particles and {001}/{101} crystal facets could be found obviously in other samples. In addition, some nanoparticles had defects or pores on the surface, which further reduced the consistency of the morphology. In previous studies [21–24], TiO₂ particles had good consistency, uniform particle size and obvious crystal facet characteristics, which were not found in T1. However, the tendency of agglomerated into micron-sized spheroid could be obtained in T1 and which did not exist in those studies. The above results indicated that although a small amount of spherical structure existed in T1, the concentration of 0.0667 mol/L NaF was insufficient for the formation of consistent microspheres. As the NaF concentration was increased to 0.0833 mol/L, spherical particles with co-exposed {001}/{101} crystal planes came into being and crystallinity of the crystals improved, while the crystal plane was still unclear and had many defects (Figure 2c,d). With a further increase in the NaF concentrations to 0.1 mol/L, microspheres with truncated tetragonal pyramidal TiO₂ nanocrystals were obtained almost all in spherical shape (Figure 2e,f), which disclosed that 0.1 mol/L or higher NaF concentration were appropriate for the preparation of well-dispersion microspheres (Figure S2) with co-exposed {001}/{101} crystal planes. When the NaF concentration increase to 0.1167 mol/L, the agglomeration between microspheres occurred, which led to a further increase in particle size of microspheres as well as the truncated tetragonal pyramidal single crystals that made up the microspheres (Figure 2g,h).

To explore the formation mechanism of the microspheres, the morphologies of samples hydrothermal-treated at different reaction times were investigated to speculate the evolution of the microspheres (Figure 3). As shown in Figure 3a, the dominant products after 20 min of reaction time were agglomerated particles with flower-like morphology, which had a size of 1.0 μm whereas its spindle-shaped primary particle sizes with lengths 100–400 nm and diameters in the range from 100 to 200 nm. With the extension of reaction time from 20 to 30 min, the particle size of the agglomerated particles was increased from 1 μm to 2 μm, the flower-like morphology started to be spherical, and the spindle-shaped primary particles constituting the agglomerated particles turned into a truncated bipyramids with {001} crystal plane (Figure 3b). When the reaction time was increased to 6 h (Figure 3c), all the spindle-shaped primary particles were disappeared and the size of spherical particles was about 2–3 μm in diameter, which were assembled from decahedral crystals with clear {001} crystal planes, were produced. Moreover, the sphericity and dispersibility of the product were significantly improved. With a further increase in reaction time to 12 h, the as-prepared microparticles with smooth {001}/{101} crystal planes were monodisperse, spherical and non-aggregated, it possessed a higher percentage of anatase {001} crystal planes, which should be attributed to a high-degree truncation of fluorine along the [001] axes in a longer reaction time of 12 h. In addition, no surface defects were observed in Figure 3d, it indicated that the crystallinity of the decahedral was intact, which was remarkably consistent with the XRD results of Figure 1(T3). When the reaction time was further increased to 24 h, due to the intensified etching of F ions, a few surfaces of

truncated bipyramid constituting the microspheres became rough and porous (Figure 3e). Meanwhile, the particle size and dispersibility of the microspheres were almost unchanged.

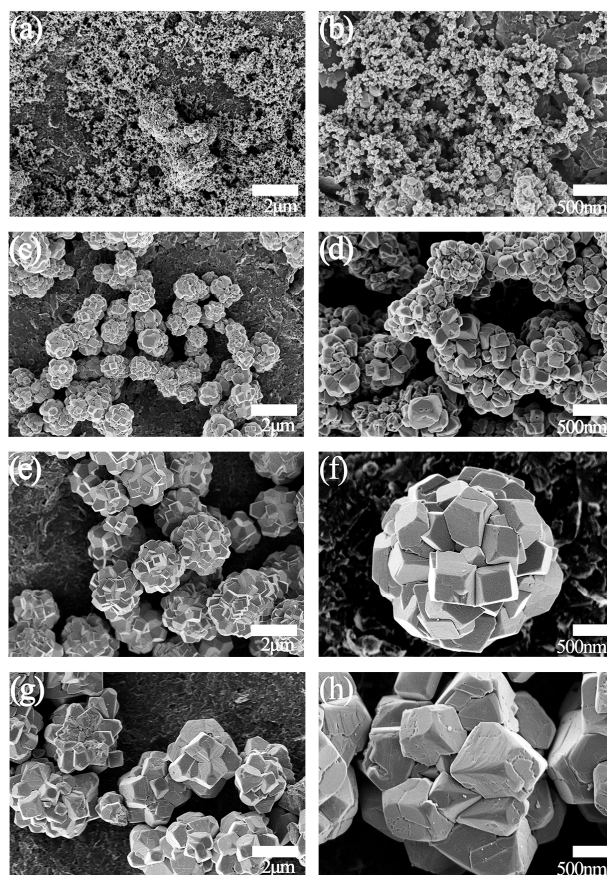


Figure 2. Field emission scanning electron microscopy images of the samples synthesized for 12 h at different NaF concentrations: (a,b) T1; (c,d) T2; (e,f) T3; (g,h) T4.

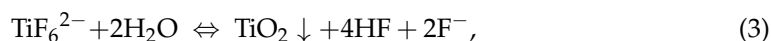
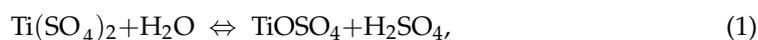
2.2. BET Analysis

The N_2 adsorption–desorption isotherm of the obtained samples is shown in Figure 4a. It could be seen that the isotherms of T1, T2, T3 and T4 were all typical type IV curves with a type H3 hysteric loop, which indicated the characteristic of material with crevice.

Furthermore, Figure 4b showed the BET surface areas of the samples. It could be seen from Figure 4b that all the surface areas of samples T2, T3 and T4 were smaller than that of T1, owing to the enlargement in particle size resulted in a corresponding decrease in the specific surface area from 37.2 to 5.1 m^2/g , which was also consistent with SEM images in Figure 2.

2.3. Growth Mechanism

As in the above-mentioned results, the influence of NaF concentration on the growth of TiO_2 microspheres was investigated. Accordingly, a possible specific formation mechanism of the microspheres was proposed. During the preparation, the cumulative hydrolysis reaction and formation of titanium oxide precipitates can be described as follows [18,31–35]:



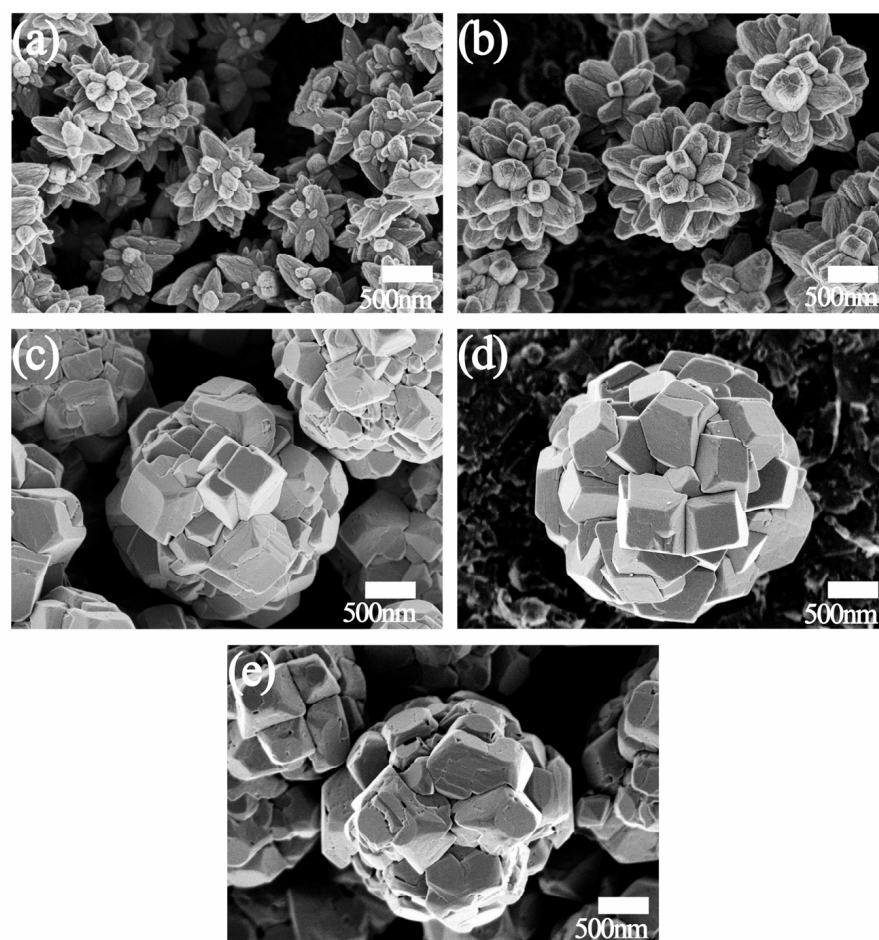


Figure 3. Field emission scanning electron microscopy images of the samples synthesized by varying the reaction duration at (a) 20 min, (b) 30 min, (c) 6 h, (d) 12 h, and (e) 24 h, keeping other parameters fixed (e.g. reaction temperature, NaF concentrations and $\text{Ti}(\text{SO}_4)_2$).

At the primary stage of the reaction, a large number of titanium oxide crystal nuclei were formed and gradually grown into nanocrystals, and these nanocrystals tended to aggregate and turned into larger nanocrystals. Then, the dissolution of small nanocrystals and the re-deposition of the dissolved species on the surfaces of the larger nanocrystals led to a rapid growth along [001] direction, driven by the relatively high surface energy of {001} surface [36]. Therefore, the oriented attachment between the larger nanocrystals results in the appearance of the spindle-shaped particles. In order to reduce the total surface energy, some nanocrystals tend to adsorb on the {010} crystal plane of the spindle-like particles and grow further due to the oriented attachment [37]. Based on Ostwald ripening, the {010} crystal planes gradually disappear, and the spindle-like crystals develop into incomplete flower-like spheres. During the Ostwald ripening and oriented attachment process, the recrystallization was modified by the presence of F ions, which was the reason that decahedrons came into being [10,38,39]. However, low F ion concentration was not enough to stabilize {001} crystal planes, so the {001} crystal surfaces were few and the interface was not clear [31]. With the increase in NaF concentration, the more F ion stabilized {001} surfaces, the more {001} surfaces appearance, thus the appearance of microspheres with better dispersion and exposed {001} planes could be observed during the consecutive dissolution–recrystallization process. However, the surface of the microspheres can be etched to produce defects if the concentration of F ion is high. Therefore, the appropriate concentration of F ions can be conducive to the formation of microspheres. The formation mechanism of microspheres is shown in Figure 5.

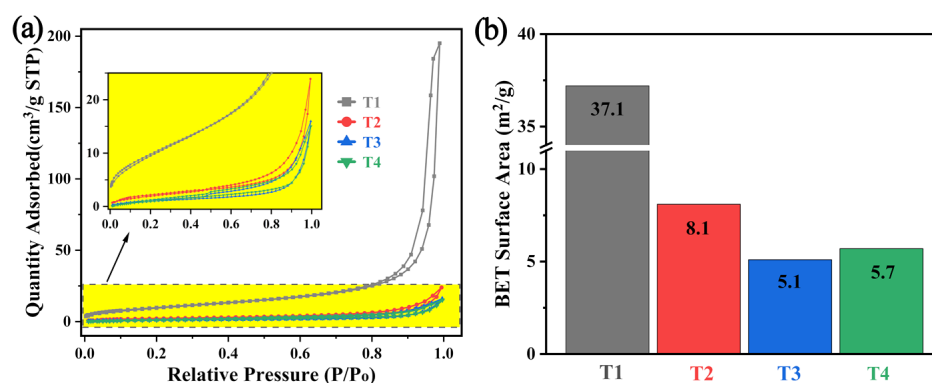


Figure 4. (a) N_2 adsorption–desorption isotherms of samples, (b) BET surface areas of samples.

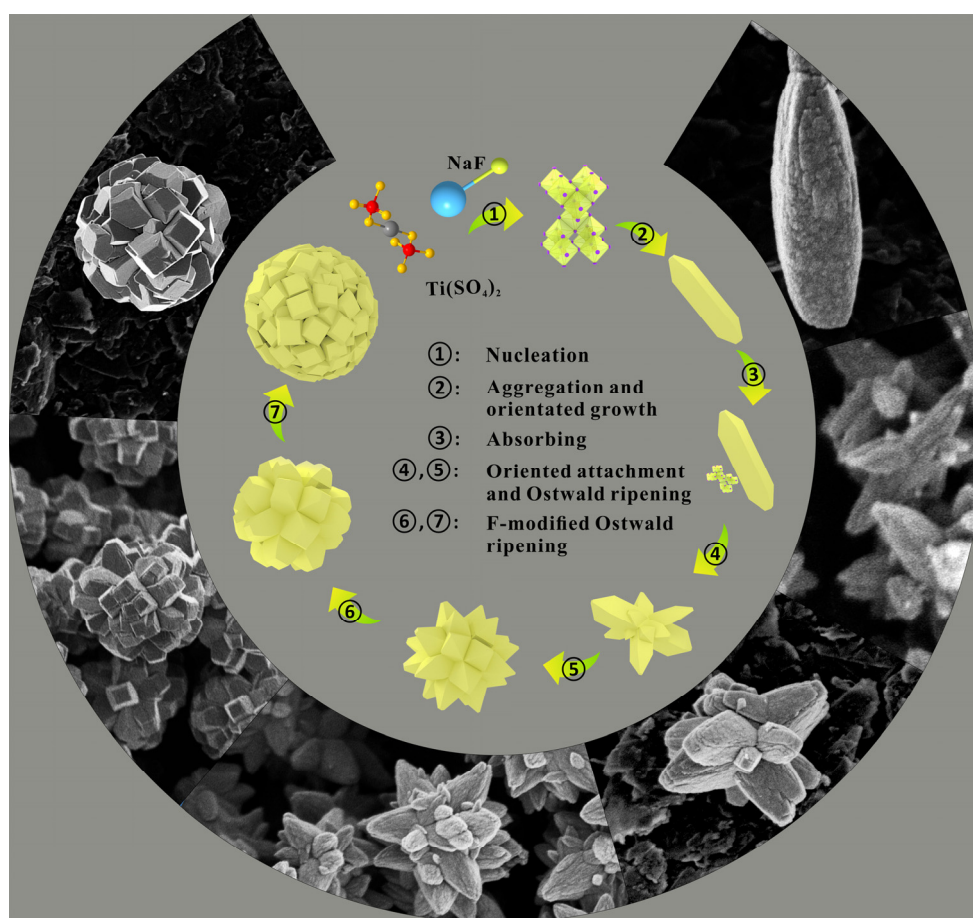


Figure 5. The formation mechanism of microspheres.

2.4. Photocatalytic Activity Evaluation

The photocatalytic activity of the as-prepared samples on TC degradation is shown in Figure 6, T1 had the best photocatalytic activity among these four samples possibly due to its smallest particle size, since smaller particle size means a larger specific surface area (as shown in Figure 4) and could provide more active sites for the reaction. Compared with T1, the photocatalytic activities of T2 and T3 were decreased gradually by decreasing the specific surface area. Although the specific surface area of T4 was larger than that of T3, the photocatalytic activity of T4 was the worst due to the easily recombination of photogenerated electron/hole pairs which was caused by the surface defects formed by F ion etching. For T3, on the premise of maintaining certain photocatalytic activity, its

larger particle size increases its recoverability. Compared with P25, T3 could completely self-precipitated within 4 h, which is impossible for nanoparticles (as shown in Figure S3).

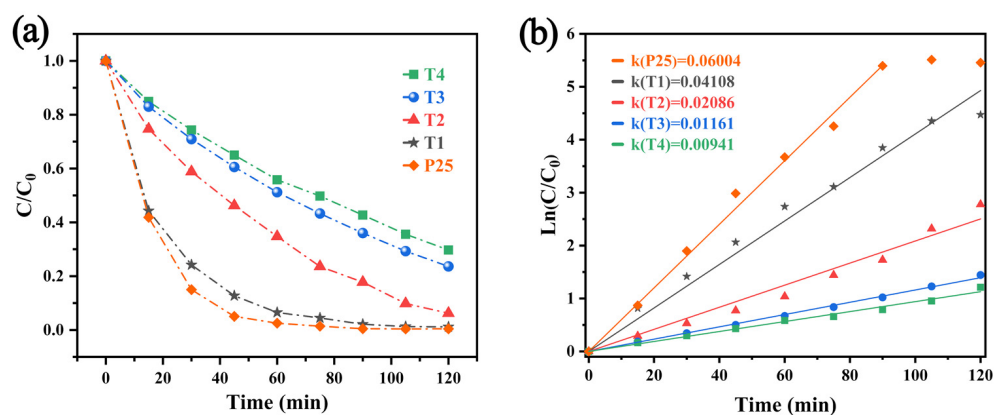


Figure 6. Photocatalytic activity: (a) degradations of Tetracycline hydrochloride, (b) kinetic linear fitting curves.

The photocatalytic mechanism of co-exposed {001}/{101} anatase TiO_2 microspheres (as shown in Figure 7) can be summarized as follows: at first, photogenerated electron-hole pairs were generated on the surface of the microspheres under photoirradiation, then the electron-hole pairs were separated spontaneously due to the crystal surface effect of anatase TiO_2 [19,40], i.e., the electrons and holes migrated to the {101} and {001} crystal surfaces, respectively (red spheres represent the holes and blue spheres represent the electrons), finally the oxidation and reduction reactions were carried out, respectively.

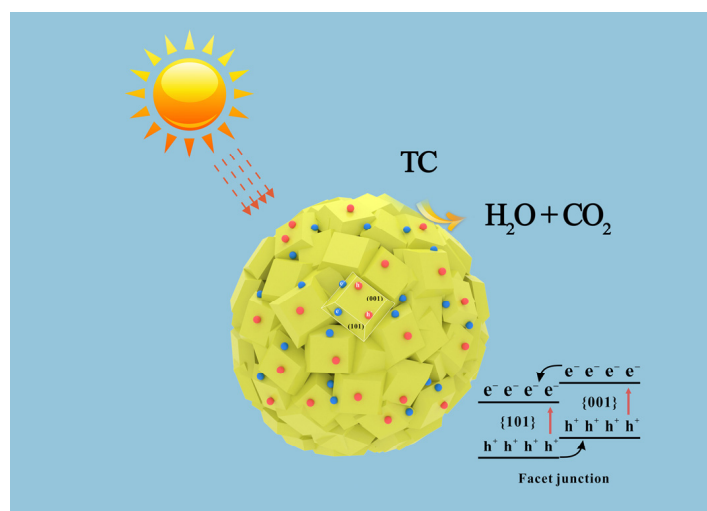


Figure 7. Schematic diagram of photocatalytic degradation mechanism.

3. Materials and Methods

3.1. Synthesis of Materials

All chemicals used in this study were without further treatment. Titanium (IV) sulfate ($\text{Ti}(\text{SO}_4)_2$, Macklin Inc purity $\geq 96\%$) was used as Ti source. Sodium fluoride (NaF, Shanghai Chemical Reagent Factory of China purity $\geq 99\%$) was used to control the morphology of the TiO_2 microspheres. To prepare the mixed aqueous solutions for synthesis of TiO_2 microspheres, 0.1680 g, 0.2099 g, 0.2519 g, and 0.2939 g of NaF was dissolved in 60 mL aqueous solutions of $\text{Ti}(\text{SO}_4)_2$ with concentrations of $0.0167 \text{ mol}\cdot\text{L}^{-1}$. The obtained powders were denoted as Samples T1, T2, T3 and T4, respectively. In a typical procedure, 0.2519 g of NaF and 0.24 g of $\text{Ti}(\text{SO}_4)_2$ were mixed in a 100 mL Teflon-lined autoclave with 60 mL of

deionized water at room temperature. After ultrasonic treating for 0.5 h, the Teflon-lined autoclave was kept at 200 °C for 12 h and cooled to room temperature naturally. Then, the white precipitate was collected and washed three times with deionized water. Finally, the TiO₂ powder was obtained by freeze-drying at −85 °C for 24 h.

3.2. Characterization of Materials

X-ray diffraction (XRD) patterns of the powders were recorded on an X-ray diffractometer (XRD, PANalytical Empyrean X-ray diffractometer, Panalytical, Almelo, Netherlands) equipped with a Cu K α radiation ($\lambda = 0.15418$ nm) source. The accelerating voltage and the applied current were 40 kV and 40 mA, the step size was 0.2°. The diffraction data were obtained over the range $10^\circ \leq 2\theta \leq 90^\circ$ (5°/min). The morphologies of the powders were analyzed by field-emission scanning electron microscopy (SEM, SU8010, Hitachi, Tokyo, Japan) operating with deceleration mode at 1 kV accelerating voltage and 10 mA applied current. Surface areas and porosities of the samples were characterized using nitrogen sorption measurements conducted at 77 K, the Brunauer–Emmett–Teller (BET) method was used to analyze the specific surface area (BET, ASAP 2020 PLUS, Micromeritics, Norcross, GA, USA).

3.3. Photocatalytic Activity Evaluation

The photocatalytic activity of the samples was evaluated by the decolorization of Tetracycline hydrochloride (TC) aqueous solutions at room temperature. Typically, 0.03 g of the as-prepared TiO₂ powder was dispersed in 100 mL of 10 mg/L TC aqueous solution in a photocatalytic reactor. Prior to irradiation, the suspension was magnetically stirred in dark condition for 30 min to reach an adsorption/desorption equilibrium. Then, the suspension was kept stirring and irradiated for different durations under a xenon lamp (300 W, 100 mW/cm²) at a working distance of 10 cm (Circulating water cooling). After every 15 min of photoirradiation, 6 mL aliquot was sampled (Medical disposable syringe 10 mL) and centrifuged (10,000 rpm, room temperature) to remove the particles, and the TC concentration was analyzed by measuring the absorption intensity using a UV-1800 UV-vis spectrophotometer (UV-vis spectrophotometer, UV-1800, Macylab, Shanghai, China). Degradation rate of TC is expressed by the following formula:

$$D_t = \frac{C_0 - C_t}{C_0}, \quad (4)$$

D_t was the degradation rate, C_0 was the concentration after adsorption/desorption equilibrium, C_t was the concentration at the duration of t .

4. Conclusions

In summary, a facile hydrothermal method was developed for preparation of anatase TiO₂ microspheres with exposed {001} facets and the possible formation mechanism of microspheres was proposed, meanwhile a new idea for controllable preparation of TiO₂ hierarchical microspheres was also provided. The as-obtained TiO₂ microspheres exhibited high photocatalytic activity on degradation of TC solution under xenon lamp irradiation. In addition, the produced microspheres have excellent crystallinity, morphology and size, which can be conducive to recycling (completely self-precipitated within 4 h) and have broad application prospects in the fields of photocatalysis and optoelectronics.

Supplementary Materials: The following supporting information can be downloaded at: <https://www.mdpi.com/article/10.3390/catal13010201/s1>, Figure S1: Higher magnification SEM image of T1; Figure S2: Particle size of microspheres; Figure S3: Precipitation time of microspheres (MS) and P25; Table S1: Comparison of TiO₂ photocatalytic activity in different literatures [18,21,22,27,33,38,41,42]; Table S2: Crystallinity of different sample.

Author Contributions: Conceptualization, Z.W.; methodology, K.W., Z.W. and Y.C.; investigation, H.H.; resources, Y.C. and Z.W.; writing—original draft preparation, H.H. and Q.K.; writing—review and editing, H.H. and X.Y.; visualization, H.H.; supervision, Y.C. and Z.W.; funding acquisition, Y.C. and Z.W. All authors have read and agreed to the published version of the manuscript.

Funding: This work was supported by the National Natural Science Foundation of China (NSFC) (51802087 and 51004046), the Natural Science Foundation of the Hubei province of China (2019CFB524 and 2010CDB05806), and the Green Industry Leading Program of Hubei University of Technology (XJ2021002101).

Data Availability Statement: Not applicable.

Conflicts of Interest: The authors declare no conflict of interest.

References

1. Liu, T.; Zhang, H. Novel Fe-doped anatase TiO₂ nanosheet hierarchical spheres with 94%{001} facets for efficient visible light photodegradation of organic dye. *RSC Adv.* **2013**, *3*, 16255–16258. [[CrossRef](#)]
2. Ji, L.; Liu, X.; Xu, T.; Gong, M.; Zhou, S. Preparation and photocatalytic properties of carbon/carbon-doped TiO₂ double-layer hollow microspheres. *J. Sol-Gel Sci. Technol.* **2020**, *93*, 380–390. [[CrossRef](#)]
3. Xie, J.; Jiang, D.; Chen, M.; Li, D.; Zhu, J.; Lü, X.; Yan, C. Preparation and characterization of monodisperse Ce-doped TiO₂ microspheres with visible light photocatalytic activity. *Colloids Surf. A Physicochem. Eng. Asp.* **2010**, *372*, 107–114. [[CrossRef](#)]
4. Akple, M.S.; Low, J.; Qin, Z.; Wageh, S.; Al-Ghamdi, A.A.; Yu, J.; Liu, S. Nitrogen-doped TiO₂ microspheres with enhanced visible light photocatalytic activity for CO₂ reduction. *Chin. J. Catal.* **2015**, *36*, 2127–2134. [[CrossRef](#)]
5. Wang, W.; Liu, Y.; Qu, J.; Chen, Y.; Shao, Z. Nitrogen-doped TiO₂ microspheres with hierarchical micro/nanostructures and rich dual-phase junctions for enhanced photocatalytic activity. *RSC Adv.* **2016**, *6*, 40923–40931. [[CrossRef](#)]
6. Park, B.-G. Photocatalytic Activity of TiO₂-Doped Fe, Ag, and Ni with N under Visible Light Irradiation. *Gels* **2021**, *8*, 14. [[CrossRef](#)]
7. Wang, A.; Wu, S.; Dong, J.; Wang, R.; Wang, J.; Zhang, J.; Zhong, S.; Bai, S. Interfacial facet engineering on the Schottky barrier between plasmonic Au and TiO₂ in boosting the photocatalytic CO₂ reduction under ultraviolet and visible light irradiation. *Chem. Eng. J.* **2021**, *404*, 127145. [[CrossRef](#)]
8. Wanbayor, R.; Ruangpornvisuti, V. A periodic DFT study on binding of Pd, Pt and Au on the anatase TiO₂ (0 0 1) surface and adsorption of CO on the TiO₂ surface-supported Pd, Pt and Au. *Appl. Surf. Sci.* **2012**, *258*, 3298–3301. [[CrossRef](#)]
9. Meng, A.; Zhang, J.; Xu, D.; Cheng, B.; Yu, J. Enhanced photocatalytic H₂-production activity of anatase TiO₂ nanosheet by selectively depositing dual-cocatalysts on {101} and {001} facets. *Appl. Catal. B Environ.* **2016**, *198*, 286–294. [[CrossRef](#)]
10. Shi, Z.; Lin, L.; Chen, R.; Yan, L. Adsorption of CO molecules on anatase TiO₂(001) loaded with noble metals M (M = Ir/Pd/Pt): A study from DFT calculations. *Mater. Today Commun.* **2021**, *28*, 102699. [[CrossRef](#)]
11. Tong, R.; Liu, C.; Xu, Z.; Kuang, Q.; Xie, Z.; Zheng, L. Efficiently Enhancing Visible Light Photocatalytic Activity of Faceted TiO₂ Nanocrystals by Synergistic Effects of Core-Shell Structured Au@CdS Nanoparticles and Their Selective Deposition. *ACS Appl. Mater. Interfaces* **2016**, *8*, 21326–21333. [[CrossRef](#)] [[PubMed](#)]
12. Hu, K.; Lei, E.; Hu, C.; Zhao, D.; Zhu, M.; Wang, J.; Zhao, W. gC₃N₄/TiO₂ composite microspheres: In situ growth and high visible light catalytic activity. *CrystEngComm* **2020**, *22*, 7104–7112. [[CrossRef](#)]
13. Ma, Y.; Zhang, C.; Li, C.; Qin, F.; Wei, L.; Hu, C.; Hu, Q.; Duo, S. Nanoscaled Bi₂O₄ confined in firework-shaped TiO₂ microspheres with enhanced visible light photocatalytic performance. *Colloids Surf. A Physicochem. Eng. Asp.* **2019**, *580*, 123757. [[CrossRef](#)]
14. Wang, W.S.; Wang, D.H.; Qu, W.G.; Lu, L.Q.; Xu, A.W. Large ultrathin anatase TiO₂ nanosheets with exposed {001} facets on graphene for enhanced visible light photocatalytic activity. *J. Phys. Chem. C* **2012**, *116*, 19893–19901. [[CrossRef](#)]
15. Cheng, B.; Le, Y.; Yu, J. Preparation and enhanced photocatalytic activity of Ag@TiO₂ core-shell nanocomposite nanowires. *J. Hazard. Mater.* **2010**, *177*, 971–977. [[CrossRef](#)]
16. Li, G.; Chen, J.; Wu, S.; Yu, Y.; Li, Y.; Gao, J. The relationship between the mesostructure of WO₃/TiO₂ hollow microsphere and its property. *Surf. Innov.* **2017**, *6*, 37–46.
17. Shaikh, S.F.; Kwon, H.-C.; Yang, W.; Mane, R.S.; Moon, J. Performance enhancement of mesoporous TiO₂-based perovskite solar cells by ZnS ultrathin-interfacial modification layer. *J. Alloys Compd.* **2018**, *738*, 405–414. [[CrossRef](#)]
18. Yang, H.G.; Sun, C.H.; Qiao, S.Z.; Zou, J.; Liu, G.; Smith, S.C.; Cheng, H.M.; Lu, G.Q. Anatase TiO₂ single crystals with a large percentage of reactive facets. *Nature* **2008**, *453*, 638–641. [[CrossRef](#)]
19. Liu, G.; Yang, H.G.; Pan, J.; Yang, Y.Q.; Lu, G.Q.; Cheng, H.-M. Titanium Dioxide Crystals with Tailored Facets. *Chem. Rev.* **2014**, *114*, 9559–9612. [[CrossRef](#)]
20. Sun, J.; Sun, J.; Wang, X. Anatase TiO₂ with Co-exposed (001) and (101) Surface-Based Photocatalytic Materials for Energy Conversion and Environmental Purification. *Chem.-Asian J.* **2020**, *15*, 4168–4183. [[CrossRef](#)]
21. Li, H.; Zeng, Y.; Huang, T.; Piao, L.; Liu, M. Controlled synthesis of anatase TiO₂ single crystals with dominant {001} facets from TiO₂ powders. *ChemPlusChem* **2020**, *77*, 1017–1021. [[CrossRef](#)]

22. Liu, M.; Piao, L.; Zhao, L.; Ju, S.; Yan, Z.; He, T.; Zhou, C.; Wang, W. Anatase TiO₂ single crystals with exposed {001} and {110} facets: Facile synthesis and enhanced photocatalysis. *Chem. Commun.* **2010**, *46*, 1664–1666. [[CrossRef](#)] [[PubMed](#)]
23. Yu, J.; Low, J.; Xiao, W.; Zhou, P.; Jaroniec, M. Enhanced photocatalytic CO₂-reduction activity of anatase TiO₂ by coexposed {001} and {101} facets. *J. Am. Chem. Soc.* **2014**, *136*, 8839–8842. [[CrossRef](#)] [[PubMed](#)]
24. Li, J.; Xu, D. Tetragonal faceted-nanorods of anatase TiO₂ single crystals with a large percentage of active {100} facets. *Chem. Commun.* **2010**, *46*, 2301–2303. [[CrossRef](#)] [[PubMed](#)]
25. Pan, J.; Wu, X.; Wang, L.; Liu, G.; Lu, G.Q.M.; Cheng, H.M. Synthesis of anatase TiO₂ rods with dominant reactive {010} facets for the photoreduction of CO₂ to CH₄ and use in dye-sensitized solar cells. *Chem. Commun.* **2011**, *47*, 8361–8363. [[CrossRef](#)] [[PubMed](#)]
26. Xiang, Q.; Yu, J.; Jaroniec, M. Tunable photocatalytic selectivity of TiO₂ films consisted of flower-like microspheres with exposed {001} facets. *Chem. Commun.* **2011**, *47*, 4532–4534. [[CrossRef](#)]
27. Han, S.; Niu, Q.; Qin, N.; Gu, X.; Zhang, Y.N.; Hua, G. In situ growth of M-{001} TiO₂/Ti photoelectrodes: Synergetic dominant {001} facets and ratio-optimal surface junctions for the effective oxidation of environmental pollutants. *Chem. Commun.* **2020**, *56*, 1337–1340. [[CrossRef](#)]
28. Sayed, M.; Shah, L.A.; Khan, J.A.; Shah, N.S.; Nisar, J.; Khan, H.M.; Zhang, P.; Khan, A.R. Efficient photocatalytic degradation of norfloxacin in aqueous media by hydrothermally synthesized immobilized TiO₂/Ti films with exposed {001} facets. *J. Phys. Chem. A* **2016**, *120*, 9916–9931. [[CrossRef](#)]
29. Zheng, Z.; Huang, B.; Lu, J.; Qin, X.; Zhang, X.; Dai, Y. Hierarchical TiO₂ microspheres: Synergetic effect of {001} and {101} facets for enhanced photocatalytic activity. *Chem. Eur. J.* **2011**, *17*, 15032–15038. [[CrossRef](#)]
30. Shaikh, S.F.; Mane, R.S.; Min, B.K.; Hwang, Y.; Joo, J.O.S. D-sorbitol-induced phase control of TiO₂ nano-particles and its application for dye-sensitized solar cells. *Sci. Rep.* **2016**, *6*, 20103. [[CrossRef](#)]
31. Baes, C.F., Jr.; Mesmer, R.E. Thermodynamics of cation hydrolysis. *Am. J. Sci.* **1981**, *281*, 935–962. [[CrossRef](#)]
32. Hong, H.-J.; Ban, G.; Lee, S.-M.; Park, I.-S.; Lee, Y.-J. Synthesis of 3D-structured Li₄Ti₅O₁₂ from titanium(IV) oxysulfate (TiOSO₄) solution as a highly sustainable anode material for lithium-ion batteries. *J. Alloys Compd.* **2020**, *844*, 156203. [[CrossRef](#)]
33. Fu, X.; Fan, C.; Yu, S.; Shi, L.; Wang, Z. TiO₂ mesocrystals with exposed {001} facets as efficient photocatalysts. *J. Alloy Compd.* **2016**, *680*, 80–86. [[CrossRef](#)]
34. Xu, M.; Ruan, P.; Xie, H.; Yu, A.; Zhou, X. Mesoporous TiO₂ Single-Crystal Polyhedron-Constructed Core-Shell Microspheres: Anisotropic Etching and Photovoltaic Property. *ACS Sustain. Chem. Eng.* **2014**, *2*, 621–628. [[CrossRef](#)]
35. Xiao, J.; Li, P.; Wen, X. Alkali-corrosion synthesis and excellent DSSC performance of novel jujube-like hierarchical TiO₂ microspheres. *Nanotechnology* **2018**, *29*, 175603. [[CrossRef](#)] [[PubMed](#)]
36. Lazzeri, M.; Vittadini, A.; Selloni, A. Structure and energetics of stoichiometric TiO₂ anatase surfaces. *Phys. Rev. B* **2001**, *63*, 155409. [[CrossRef](#)]
37. Li, D.; Nielsen, M.H.; Lee, J.R.I.; Frandsen, C.; Banfield, J.F.; De Yoreo, J.J. Direction-Specific Interactions Control Crystal Growth by Oriented Attachment. *Science* **2012**, *336*, 1014–1018. [[CrossRef](#)]
38. Wang, L.; Xie, Y.; Liu, W.; Wang, Q.; Cao, W. Synthesis of mesoporous core-shell TiO₂ microstructures with coexposed {001}/{101} facets: Enhanced intrinsic photocatalytic performance. *Environ. Sci. Pollut. Res.* **2018**, *25*, 31250–31261. [[CrossRef](#)]
39. Liu, G.; Yu, J.C.; Lu, G.Q.; Cheng, H.-M. Crystal facet engineering of semiconductor photocatalysts: Motivations, advances and unique properties. *Chem. Commun.* **2011**, *47*, 6763–6783. [[CrossRef](#)]
40. Tachikawa, T.; Yamashita, S.; Majima, T. Evidence for Crystal-Face-Dependent TiO₂ Photocatalysis from Single-Molecule Imaging and Kinetic Analysis. *J. Am. Chem. Soc.* **2011**, *133*, 7197–7204. [[CrossRef](#)]
41. Cai, J.; Wang, Z.; Lv, K.; Zheng, Y.; Yu, J.; Li, M. Rapid synthesis of a TiO₂ hollow microsphere assembly from hollow nanoparticles with enhanced photocatalytic activity. *RSC Adv.* **2013**, *3*, 15273–15281. [[CrossRef](#)]
42. Wei, T.; Niu, B.; Zhao, G. Highly characteristic adsorption based on single crystal {001}-TiO₂ surface molecular recognition promotes enhanced oxidation. *ACS Appl. Mater. Interfaces* **2020**, *12*, 39273–39281.

Disclaimer/Publisher's Note: The statements, opinions and data contained in all publications are solely those of the individual author(s) and contributor(s) and not of MDPI and/or the editor(s). MDPI and/or the editor(s) disclaim responsibility for any injury to people or property resulting from any ideas, methods, instructions or products referred to in the content.